JOURNAL OF Applied Polymer SCIENCE

MesoDyn Simulation Study on the Phase Morphologies of Miktoarm PS-*b*-PMMA Copolymer Doped by Nanoparticles

Dan Mu,[1] Jian-Quan Li,[2] Song Wang[3]

[1]College of Chemistry Chemical Engineering and Materials Science, Zaozhuang University, Shandong 277160, People's Republic of China

[2]Opto-Electronic Engineering College, Zaozhuang University, Shandong 277160, People's Republic of China

[3]Institute of Theoretical Chemistry, State Key Laboratory of Theoretical and Computational Chemistry, Jilin University, Changchun 130023, People's Republic of China

Correspondence to: D. Mu (E-mail: mudanjlu1980@yahoo.com.cn)

ABSTRACT: The compatibility of six groups 12 miktoarm polystyrene-block-poly(methyl methacrylate) copolymers is studied at 383, 413, and 443 K via mesoscopic modeling. The values of the order parameters depend on both the architectures of the block copolymers and the simulation temperature, whereas the change tendency of the order parameters is nearly the same at 413 and 443 K. Obviously, temperature presents more obvious effect on long and PMMA-rich chains. A study of plain copolymers doped with nanoparticles shows that the microscopic phase is influenced by not only the properties of the nanoparticles, such as the size, number, and density, but also by the composition and architecture of copolymers. Increasing the size and the number of the nanoparticles used as a dopant plays the most significant role on the phase morphologies of the copolymers at lower and higher temperatures, respectively. Especially, the 13214-type copolymers, which are PMMA-rich composition, present microscopic phase separation as varying degrees of lamellar phase morphologies at 443 K, alternated with PS and PMMA component. © 2012 Wiley Periodicals, Inc. J. Appl. Polym. Sci. 000: 000–000, 2012

KEYWORDS: PS-*b*-PMMA copolymer; miktoarm; inducing effect; nanoparticle; phase morphology

Received 20 November 2011; accepted 13 February 2012; published online 00 Month 2012
DOI: 10.1002/app.37510

INTRODUCTION

As a fertile source of soft materials, block copolymers attract researchers in both academic and application fields because they have novel properties resulted from their self-organized microphase-separation structures.[1] The synthesis of a block copolymer with a unique architecture, such as star, comb, and ring shape, makes it possible to diversify its applications and investigate the effect of the chain architecture on its physical properties.[2] Thin films formed by block copolymers with well-defined nanostructures have received considerable attention owing to their potential nanofabrication applications.[3–10] In these applications, the ability to control the morphology of the block copolymer thin film by adjusting various influential factors to obtain an ordered phase-separated microdomain has potential significance.

Mesoscopic dynamic (MesoDyn) models have been receiving increasing attention, as they form a bridge between microscale and macroscale properties.[11–14] Compared with atomistic simulation methods, the mesoscopic dynamics[15–17] can make the scale of the simulation large by several orders of magnitude, which can deal with the polymer chain at a mesoscopic level by grouping atoms together and then coarse graining them to be persistent length polymer chains. It utilizes dynamic mean-field density functional theory (DFT), in which the dynamics of phase separation can be described by Langevin-type equations to investigate polymer diffusion. As a useful simulation technique for fluids, MesoDyn has been successfully applied to study the microphase separation of block copolymers in our former researches.[18–22]

Polystyrene (PS)/poly(methyl methacrylate)PMMA binary blends is a well-known immiscible combination,[23–30] and can be observed bulk and surface phase separation.[31,32]

Polystyrene-block-poly(methyl methacrylate) (PS-*b*-PMMA) copolymer is a polymer composed of two immiscible polymers blocks, which was studied in our former study; we had obtained the representative chain lengths of PS and PMMA chain, the χ data of 10 different compositions which can cover most compositions at 383, 413, and 443 K,[20] and these data could be applied as the input parameters to deal with the PS-*b*-PMMA

Applied Polymer SCIENCE

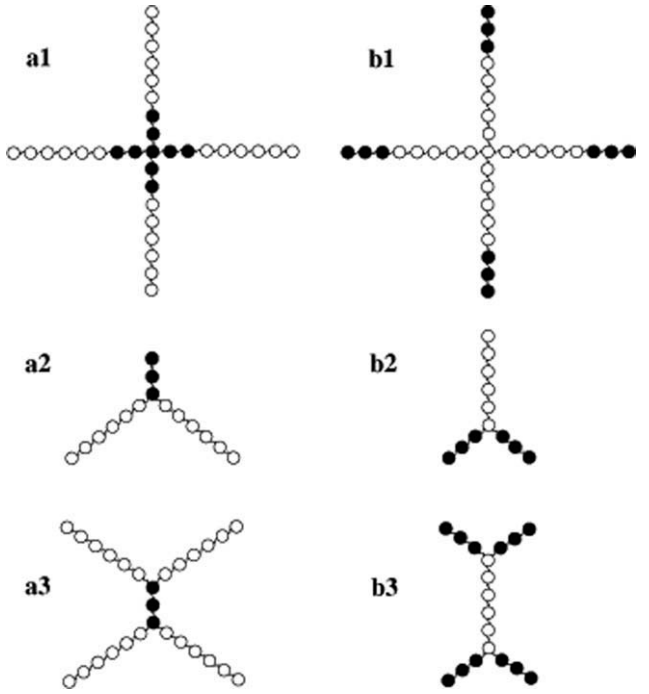

Figure 1. The schematic miktoarm PS-*b*-PMMA copolymer models used in this study. The black particles represent the PS component denoted as A, whereas the white particles represent the PMMA component denoted as B.

copolymers in this study. Immiscible graft and block copolymers made of PS and PMMS blocks have received increasing attention owing to their potential applications in keratoprosthesis modification,[33] drug carriers,[34] and biomedical materials.[35,36] However, there are no reports on the inducing effects of nanoparticles on the miktoarm PS-*b*-PMMA copolymer. We gained some useful results in the study reported in this article that can be applied to nanofabrication to improve its function.

SIMULATION METHOD AND MODEL CONSTRUCTION

Mesoscale structures are of utmost importance during the production processes of many materials, such as polymer blends, block copolymer systems, surfactant aggregates in detergent materials, latex particles, and drug delivery systems. Our simulation processes were all carried out with the MesoDyn package in the Materials Studio commercial software provided by Accelrys on an SGI workstation. MesoDyn is a state-of-the-art mesoscale simulation program. It utilizes a dynamic variant of mean-field DFT with Langevin-type equations to investigate polymer diffusion, providing a coarse-grained method for the study of complex fluids, their kinetics, and their equilibrium structures at large length and time scales. The thermodynamic forces are found via mean-field DFT, using the Gaussian chain as a model. The coarse-grained Gaussian chain consists of beads with equal lengths and equal volumes. With time evolution, the free energy of the system results in no discernible changes, whereas the phase separation is considered completed.

We have obtained the representative chain lengths of PS and PMMA chain in our former study.[19] Therefore, the block copolymer chains are constructed by PS (denoted as "A") and PMMA (denoted as "B") components as $A(A_2B_6)_4$, $A_3(B_6)_2$, $A[A(B_6)_2]_2$, $B(B_5A_3)_4$, $B_6(A_3)_2$, and $B_4[B(A_3)_2]_2$, named as 11111, 12112, 13114, 21111, 22121, and 23141. Corresponding schematic models to these six components are shown in Figure 1, they are a1, a2, a3, b1, b2, and b3, respectively. The latter three models are the component exchange between "A" and "B" from the corresponding former three. When these six models are double large, we can gain other six models, $A(A_5B_{12})_4$, $A_6(B_{12})_2$, $A_4[A(B_{12})_2]_2$, $B(B_{11}A_6)_4$, $B_{12}(A_6)_2$, and $B_{10}[B(A_6)_2]_2$, named as 11211, 12212, 13214, 21211, 22221, and 23241, respectively. Table I lists the grouping, molar ratio of blocks, molecular architecture, symbol, and corresponding scheme in detail.

We choose the nanoparticles in column shape for more inducing factors, such as the size, number, and density. The details about seven arrangements of designed doped nanoparticles arrangement are summarized in Table II; it involves the number of nanoparticles in each layer (N_p), the radius of each nanoparticle (r_p), the height of each nanoparticle (h_p), the number of layers (N_L), and the total number of nanoparticles added as dopant (N_{tp}). They are also shown in Figure 2. The 4-3-4-2 arrangement, with four nanoparticles in each layer, a nanoparticle radius of 3 nm, a nanoparticle height of 4 nm, and two

Table I. The Molecular Information of Miktoarm PS-*b*-PMMA Copolymer

Group number	Molar ratio of A5–B6	Architecture	Symbol	Scheme in Figure 1
Group 1	1 : 1	$A(A_2B_6)_{4s}$	11111	a1
		$A(A_5B_{12})_4$	11211	
Group 2	1 : 2	$A_3(B_6)_2$	12112	a2
		$A_6(B_{12})_2$	12212	
Group 3	1 : 4	$A[A(B_6)_2]_2$	13114	a3
		$A_4[A(B_{12})_2]_2$	13214	
Group 4	1 : 1	$B(B_5A_3)_4$	21111	b1
		$B(B_{11}A_6)_4$	21211	
Group 5	2 : 1	$B_6(A_3)_2$	22121	b2
		$B_{12}(A_6)_2$	22221	
Group 6	4 : 1	$B_4[B(A_3)_2]_2$	23141	b3
		$B_{10}[B(A_6)_2]_2$	23241	

Table II. The Information of Doped Nanoparticles

System	N_p	r_p (nm)	h_p (nm)	N_L	N_{tp}
4-3-4-2	4	3	4	2	8
4-3-4-3	4	3	4	3	9
4-3-4-4	4	3	4	4	16
4-3-8-2	4	3	8	2	8
4-3-8-3	4	3	8	3	9
4-6-8-2	4	6	8	2	8
8-3-4-2	8	3	4	2	16

layers, is set as the basic reference; that is, the other six are derived from it. Adding one more nanoparticle to the center of the base case yields 4-3-4-3 arrangement; increasing the number of layers to four without changing any other settings produces 4-3-4-4 arrangement; doubling the nanoparticle height leads to 4-3-8-2 arrangement; adding one more nanoparticle to the middle of the simulation box in 4-3-8-2 to increase the number of layers to three gains 4-3-8-3 arrangement; doubling the nanoparticle radius in 4-3-8-2 produces 4-6-8-2 arrangement; and doubling the nanoparticle density of every layer in 4-3-4-2 yields 8-3-4-2 arrangement. The 12 miktoarm PS-*b*-PMMA copolymers constructed above (11111, 11211, 12112, 12212, 13114, 13214, 21111, 21211, 22121, 22221, 23141, and 23241) are modeled with the inducing effect of each nanoparticle arrangement. Thus, the main objective of modeling these cases is to determine the factor that exerted the most influence on phase separation: the size, the number, the density, or the arrangement of the nanoparticles. However, we also explored the effect of varying the temperature on the phase separation.

SIMULATION RESULTS AND DISCUSSION

We start the simulations by placing the block copolymers randomly in the simulation box, followed by an equilibration of 10 ms until the free-energy density (*RT*/volume) reaches a relative stable value. The time step is set as 50 ns to stabilize the numerical calculations. The noise parameter value is 75.002, by default, is used for the numerical speed and stability. The adopted grid dimensions are 32 × 32 ×32 nm^3, and the size of the mesh over which density variations are to be plotted in MesoDyn length 1 nm.

The Flory–Huggins interaction parameter, χ data of 10 different compositions which can cover most composition at 383, 413, and 443 K,[19] and these data can be applied as the input parameters to deal with the miktoarm PS-*b*-PMMA copolymer in this study. The connection between the microscale and the mesoscale is as follows:

$$\mathrm{IPM} = \chi_{ab} RT$$

where the parameter χ_{ab} is calculated by atomistic simulation for each blend composition at different temperatures. R is the molar gas constant, 8.314 J mol^{-1} K^{-1}, and T is the simulation temperature. IPM is the abbreviation of "Input Parameter of MesoDyn" used to describe the interaction between beads.

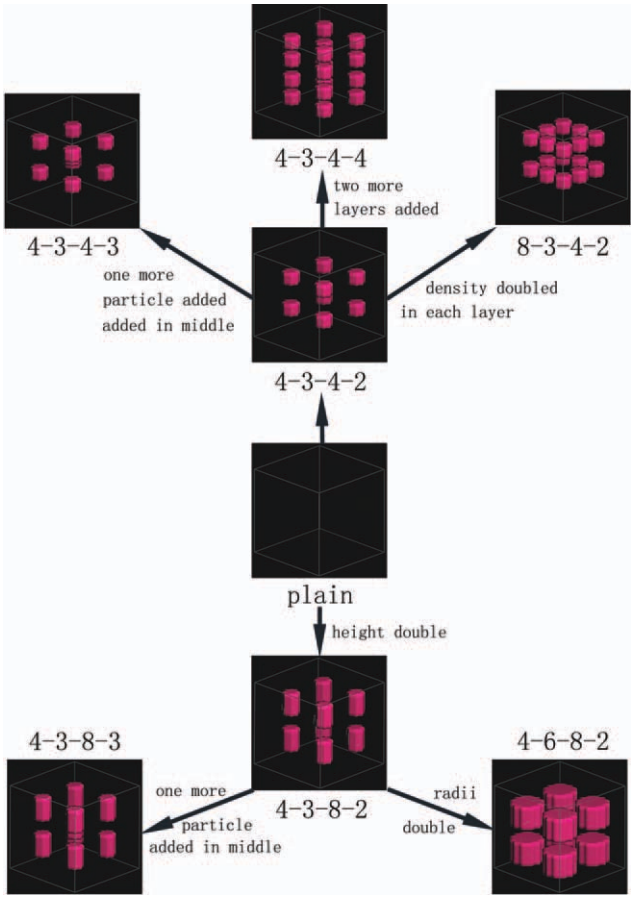

Figure 2. The scheme of seven kinds of nanoparticle arrangements. [Color figure can be viewed in the online issue, which is available at wileyonlinelibrary.com.]

The order parameter, P, is defined as the average volume of the difference between local density squared and the overall density squared, as given by the following equation

$$P_i = \frac{1}{V}\int_V [\eta_i^2(r) - \eta_i^2]\, dr$$

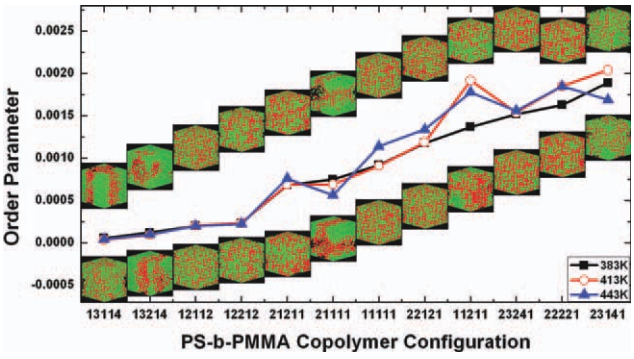

Figure 3. *P*-values of 12 miktoarm PS-*b*-PMMA copolymers at 383, 413, and 443 K. Red represents PS component; green PMMA. The isodensity surfaces of these copolymers at 383 and 413 K are displayed at the top and bottom, respectively. [Color figure can be viewed in the online issue, which is available at wileyonlinelibrary.com.]

Applied Polymer SCIENCE

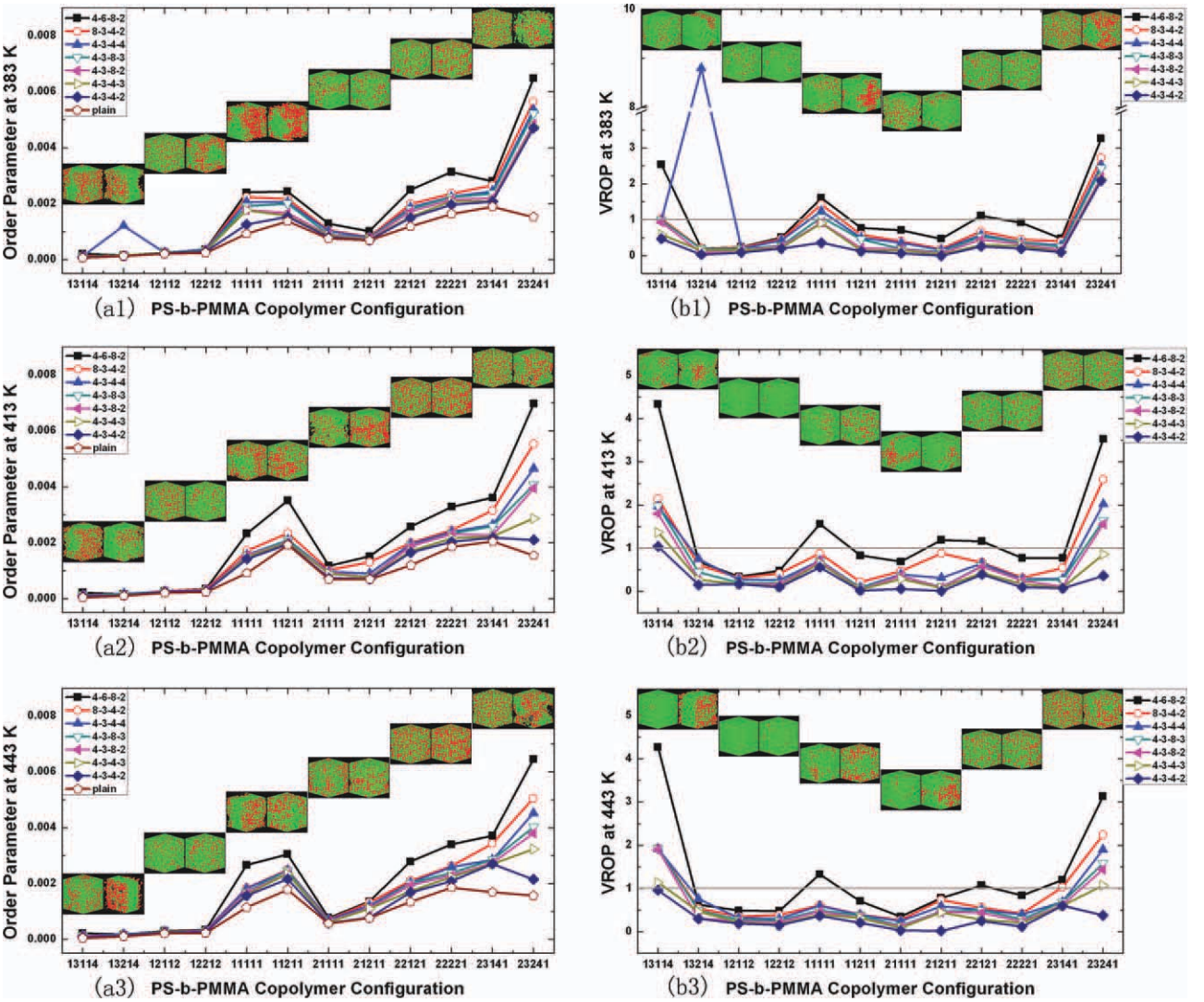

Figure 4. *P*- and VROP values of 12 miktoarm PS-*b*-PMMA copolymers doped with seven kinds of nanoparticles at 383, 413, and 443 K, respectively. The isodensity surfaces on the top of three subfigures a1, a2, and a3 are the copolymers induced by 4-3-4-3 nanoparticle effects at 383, 413, and 443 K; the isodensity surfaces on the top of three subfigures b1, b2, and b3 are the copolymers induced by 4-3-8-3 nanoparticle effects at 383, 413, and 443 K. [Color figure can be viewed in the online issue, which is available at wileyonlinelibrary.com.]

where η_i is dimensionless density for species *i*. The larger the value of the order parameter is, the more obvious the phase separation is. A decrease in *P* indicated better compatibility or miscibility, and the polymer phases mixed more randomly.

We define a new parameter to describe the inducing effect of doped nanoparticles. The order parameter value of every undoped ("plain") miktoarm PS-*b*-PMMA copolymer is named as "*a*"; in addition, the order parameter value of the corresponding copolymer with nanoparticle inducing effect is named as "*b*." The value of $(b - a)/a$ is defined as variation rates of order parameter (VROP). By comparing the VROP values, we can figure out the effective factor of doped nanoparticles on changing the phase morphology of miktoarm PS-*b*-PMMA copolymer, it is the size, density, or the arrangement. The larger the value of VROP, the greater the inducing influence.

Modeling Plain Miktoarm PS-*b*-PMMA Copolymer

Figure 3 shows the *P*-values of the 12 plain PS-*b*-PMMA copolymers at 383, 413, and 443 K. There are several features of this figure that are worth noting:

1. The order of *P*-values at 413 and 443 K is nearly the same, except 23141-type copolymer, but it changes at 383 K. The *P*-values of the PS-*b*-PMMA copolymers at 443 K are higher than the *P*-values at 383 and 413 K for the same copolymer type, except 21111-, 11211-, and 23141-type copolymers, which all have four PS blocks and are long- and short-chain copolymers in Groups 4, 1, and 6, respectively. This could be owing to the differences in compatibilities of the PS and PMMA component at different temperatures. Especially, for it at high temperature, such as 443 K could present microscopic phase separation easily.

2. The *P*-values of 13114-, 13214-, 12112-, and 12212-type PS-*b*-PMMA copolymers at 383, 413, and 443 K are nearly the same. The 13114- and 13214-type copolymers belong to Group 3, whose block ratio is 1 : 4 (PS to PMMA), in addition, 12112-, 12212-type copolymers belong to Group 2, whose block ratio is 1 : 2 (PS to PMMA). Combined with the isodensity surfaces showed, it suggests that when the copolymer with the same architecture, long, or short-chain copolymer could present nearly the same *P*-values, especially for the copolymer rich in PMMA blocks. The diffusion rate of PMMA is higher than PS, and hence the PMMA-rich copolymers would move much faster and congregate with the same blocks more easily.
3. The *P*-value of 23141-type copolymer at 383 K presents the highest, which belongs to Group 6 with block ratio of 4 : 1 (PS to PMMA); the same as it is at 413 K; but it presents the highest for 22221-type copolymer at 443 K, which belongs to Group 5 with block ratio of 2 : 1 (PS to PMMA). The 23141- and 22221-type copolymers are all rich in PS blocks, and their architecture are all simpler than it in Group 4, which are also PS-rich copolymers. Furthermore, it is more compact in the architecture of copolymers for 22221-type, compared with 23141-type copolymer. Therefore, it is easier to move and adjust its orientation during the phase assembling at higher temperature, such as 443 K, then the PS-rich region could be largened, and further microscopic separation could occur.

In summary, the architecture of copolymer is more vital than the chain length of copolymer on *P*-values at 383, 413, and 443 K.

Modeling Miktoarm PS-*b*-PMMA Copolymer Doped with Nanoparticles

Subfigures a1, a2, and a3 in Figure 4 show the *P*-values for the 12 miktoarm PS-*b*-PMMA copolymers doped with seven nanoparticles arrangements at 383, 413, and 443 K, respectively. Subfigures b1, b2, and b3 show the corresponding VROP values for these doped copolymers. A reference line is drawn through $R = 1$ in subfigures b1, b2, and b3. When a VROP value lies above this line, the doping can be considered to have a reinforcing effect; otherwise, the doping can be considered to have a weakening effect. Thus, the main objective of modeling these cases is to determine the factor that exerts the most influence on phase separation: the size, the number, the density, or the arrangement of the nanoparticles. In addition, we can also explore which type of miktoarm copolymer suffers the most by nanoparticles, inducing effect on changing the phase morphology. The following features of the plots are noteworthy:

1. It shows the *P*-values of copolymers with nanoparticles doped are all higher than its plain copolymers in subfigures a1, a2, and a3. It means that each type of copolymer suffers by the inducing effect of nanoparticles' doping on varying its phase morphology.
2. The general change tendency of *P*-values for the same copolymer type is $P_{4\text{-}6\text{-}8\text{-}2} > P_{8\text{-}3\text{-}4\text{-}2} > P_{4\text{-}3\text{-}4\text{-}4} > P_{4\text{-}3\text{-}8\text{-}3} > P_{4\text{-}3\text{-}8\text{-}2} > P_{4\text{-}3\text{-}4\text{-}3} > P_{4\text{-}3\text{-}4\text{-}2} > P_{\text{plain}}$ at 383, 413, and 443 K, respectively. However, the change tendency of 13114- and 13214-type copolymer is different from it, that is, $P_{4\text{-}6\text{-}8\text{-}2} > P_{8\text{-}3\text{-}4\text{-}2} > P_{4\text{-}3\text{-}8\text{-}3} > P_{4\text{-}3\text{-}4\text{-}4} > P_{4\text{-}3\text{-}8\text{-}2} > P_{4\text{-}3\text{-}4\text{-}3} > P_{4\text{-}3\text{-}4\text{-}2} > P_{\text{plain}}$ and $P_{4\text{-}3\text{-}4\text{-}4} > P_{4\text{-}6\text{-}8\text{-}2} > P_{8\text{-}3\text{-}4\text{-}2} > P_{4\text{-}3\text{-}8\text{-}3} > P_{4\text{-}3\text{-}4\text{-}3} > P_{4\text{-}3\text{-}8\text{-}2} > P_{4\text{-}3\text{-}4\text{-}2} > P_{\text{plain}}$. The reason leading to such differences in the relationship above is the outstanding architecture in such two types of copolymers. The 13114- and 13214-type copolymers containing the block ratio of 1 : 4 (PS to PMMA) have the lowest PS component content in the 12 copolymers. Furthermore, the four PMMA blocks locate outside; these are the two reasons for it, giving more opportunity to meet the same block of the other copolymers during mixing compared with other type copolymers.

The general highest *P*-value for the same nanoparticle arrangement inducing effect on different architecture copolymers is P_{23241} at 383, 413, and 443 K, respectively, but it is P_{23141} for 4-3-4-2 nanoparticle arrangement inducing effect at both 413 and 443 K. The 23141- and 23241-type copolymers containing block ratio of 4 : 1 (PS to PMMA) have the highest PS content in the 12 copolymers, and four PS blocks locate outside, which makes it congregate with the same blocks of the other copolymers easily. The 4-3-4-2 is the basic nanoparticle model, the simplest of all the nanoparticle arrangements, has the most vacancy room. High temperature could activate the activity of copolymers, combined with the large vacancy room in the simulation box; these two reasons force the copolymers to adjust their orientation further from assembling area, even from microscopic phase separation.

In summary, the 4-6-8-2 nanoparticle arrangement exerts the most influence on phase separation at all three temperatures, except on 13214-type PS-*b*-PMMA copolymer. In addition, 23241-type PS-*b*-PMMA copolymer suffers the most influence induced by all the nanoparticle arrangement inducing effect at all three temperatures, except 4-3-4-2 nanoparticle arrangement.

The order of VROP for the same architecture of copolymer with different nanoparticles inducing effect is generally the same as the order of *P* at 383, 413, and 443 K, that is, $\text{VROP}_{4\text{-}6\text{-}8\text{-}2} > \text{VROP}_{8\text{-}3\text{-}4\text{-}2} > \text{VROP}_{4\text{-}3\text{-}4\text{-}4} > \text{VROP}_{4\text{-}3\text{-}8\text{-}3} > \text{VROP}_{4\text{-}3\text{-}8\text{-}2} > \text{VROP}_{4\text{-}3\text{-}4\text{-}3} > \text{VROP}_{4\text{-}3\text{-}4\text{-}2}$, and the change tendencies of 13114- and 13214-type copolymer are the same as it in *P*, that is, $\text{VROP}_{4\text{-}6\text{-}8\text{-}2} > \text{VROP}_{8\text{-}3\text{-}4\text{-}2} > \text{VROP}_{4\text{-}3\text{-}8\text{-}3} > \text{VROP}_{4\text{-}3\text{-}4\text{-}4} > \text{VROP}_{4\text{-}3\text{-}8\text{-}2} > \text{VROP}_{4\text{-}3\text{-}4\text{-}3} > \text{VROP}_{4\text{-}3\text{-}4\text{-}2}$ and $\text{VROP}_{4\text{-}3\text{-}4\text{-}4} > \text{VROP}_{4\text{-}6\text{-}8\text{-}2} > \text{VROP}_{8\text{-}3\text{-}4\text{-}2} > \text{VROP}_{4\text{-}3\text{-}8\text{-}3} > \text{VROP}_{4\text{-}3\text{-}4\text{-}3} > \text{VROP}_{4\text{-}3\text{-}8\text{-}2} > \text{VROP}_{4\text{-}3\text{-}4\text{-}2}$. However, the order of VROP for the 22221-type copolymer at 383 K, 11211-type copolymer at 413 K, and 23141-type copolymer at 443 K does not follow the same order as they are in *P*, they are $\text{VROP}_{4\text{-}6\text{-}8\text{-}2} > \text{VROP}_{8\text{-}3\text{-}4\text{-}2} > \text{VROP}_{4\text{-}3\text{-}8\text{-}3} > \text{VROP}_{4\text{-}3\text{-}4\text{-}4} > \text{VROP}_{4\text{-}3\text{-}8\text{-}2} > \text{VROP}_{4\text{-}3\text{-}4\text{-}3} > \text{VROP}_{4\text{-}3\text{-}4\text{-}2}$, $\text{VROP}_{4\text{-}6\text{-}8\text{-}2} > \text{VROP}_{8\text{-}3\text{-}4\text{-}2} > \text{VROP}_{4\text{-}3\text{-}8\text{-}3} > \text{VROP}_{4\text{-}3\text{-}4\text{-}4} > \text{VROP}_{4\text{-}3\text{-}4\text{-}3} > \text{VROP}_{4\text{-}3\text{-}8\text{-}2} > \text{VROP}_{4\text{-}3\text{-}4\text{-}2}$ and $\text{VROP}_{4\text{-}6\text{-}8\text{-}2} > \text{VROP}_{8\text{-}3\text{-}4\text{-}2} > \text{VROP}_{4\text{-}3\text{-}8\text{-}3} > \text{VROP}_{4\text{-}3\text{-}4\text{-}4} > \text{VROP}_{4\text{-}3\text{-}8\text{-}2} > \text{VROP}_{4\text{-}3\text{-}4\text{-}3} > \text{VROP}_{4\text{-}3\text{-}4\text{-}2}$, respectively. They are three special cases resulted from peculiar architecture of copolymer at peculiar temperature.

5. All cases presenting a reinforcing effect, that is the VROP value is higher than 1, for the same architecture of copolymer induced by different nanoparticle arrangements are as follows:

Applied Polymer SCIENCE

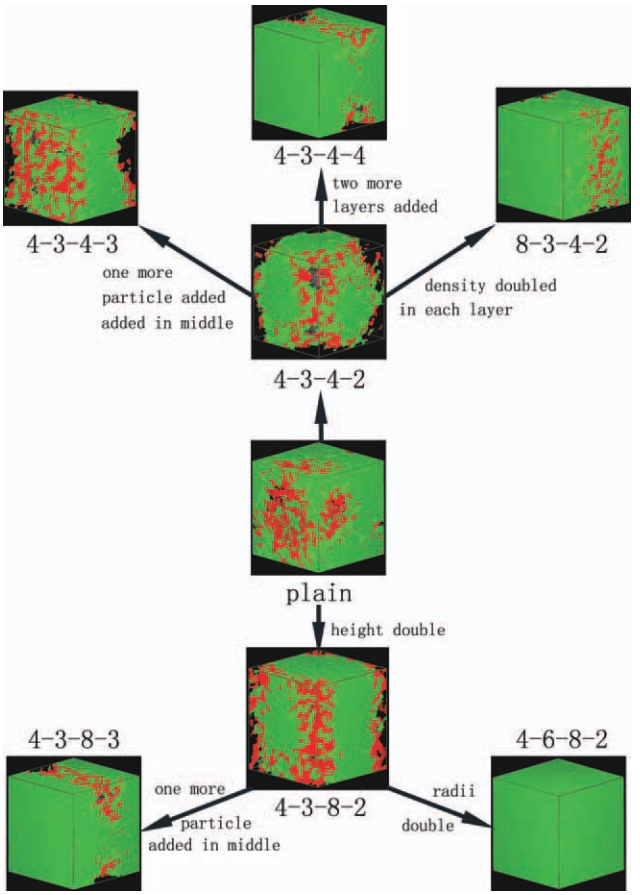

Figure 5. Isodensity surfaces of 13214-type PS-*b*-PMMA copolymer doped with seven kinds of nanoparticles at 383 K. Red represents PS component; green PMMA. [Color figure can be viewed in the online issue, which is available at wileyonlinelibrary.com.]

11111-type copolymer at 383 K, and it is in the order $VROP_{4\text{-}6\text{-}8\text{-}2} > VROP_{8\text{-}3\text{-}4\text{-}2} > VROP_{4\text{-}3\text{-}4\text{-}4} > VROP_{4\text{-}3\text{-}8\text{-}3}$; 13114-type copolymer at 383 K, and it is in the order $VROP_{4\text{-}6\text{-}8\text{-}2} > VROP_{8\text{-}3\text{-}4\text{-}2}$; 13214-type copolymer at 383 K, it is 4-3-4-4 nanoparticle arrangement; 22121-type copolymer at 383 K, it is 4-6-8-2 nanoparticle arrangement; 23241-type copolymer at 383 K, and it is in the order $VROP_{4\text{-}6\text{-}8\text{-}2} > VROP_{8\text{-}3\text{-}4\text{-}2} > VROP_{4\text{-}3\text{-}4\text{-}4} > VROP_{4\text{-}3\text{-}8\text{-}3} > VROP_{4\text{-}3\text{-}8\text{-}2} > VROP_{4\text{-}3\text{-}4\text{-}3} > VROP_{4\text{-}3\text{-}4\text{-}2}$; 11111-type copolymer at 413 K, it is 4-6-8-2 nanoparticle arrangement; 13114-type copolymer at 413 K, and it is in the order $VROP_{4\text{-}6\text{-}8\text{-}2} > VROP_{8\text{-}3\text{-}4\text{-}2} > VROP_{4\text{-}3\text{-}8\text{-}3} > VROP_{4\text{-}3\text{-}4\text{-}4} > VROP_{4\text{-}3\text{-}8\text{-}2} > VROP_{4\text{-}3\text{-}4\text{-}3} > VROP_{4\text{-}3\text{-}4\text{-}2}$; 21211-type copolymer at 413 K, it is 4-6-8-2 nanoparticle arrangement; 22121-type copolymer at 413 K, it is 4-6-8-2 nanoparticle arrangement; 23241-type copolymer at 413 K, and it is in the order $VROP_{4\text{-}6\text{-}8\text{-}2} > VROP_{8\text{-}3\text{-}4\text{-}2} > VROP_{4\text{-}3\text{-}4\text{-}4} > VROP_{4\text{-}3\text{-}8\text{-}3} > VROP_{4\text{-}3\text{-}8\text{-}2}$; 11111-type copolymer at 443 K, it is 4-6-8-2 nanoparticle arrangement; 13114-type copolymer at 443 K, and it is in the order $VROP_{4\text{-}6\text{-}8\text{-}2} > VROP_{8\text{-}3\text{-}4\text{-}2} > VROP_{4\text{-}3\text{-}8\text{-}3} > VROP_{4\text{-}3\text{-}4\text{-}4} > VROP_{4\text{-}3\text{-}8\text{-}2} > VROP_{4\text{-}3\text{-}4\text{-}3}$; 22121-type copolymer at 443 K, it is 4-6-8-2 nanoparticle arrangement; 23141-type copolymer at 443 K, and it is in the order $VROP_{4\text{-}6\text{-}8\text{-}2} > VROP_{8\text{-}3\text{-}4\text{-}2}$; 23241-type copolymer at 443 K, and it is in the order $VROP_{4\text{-}6\text{-}8\text{-}2} > VROP_{8\text{-}3\text{-}4\text{-}2} > VROP_{4\text{-}3\text{-}4\text{-}4} > VROP_{4\text{-}3\text{-}8\text{-}3} > VROP_{4\text{-}3\text{-}8\text{-}2} > VROP_{4\text{-}3\text{-}4\text{-}3}$. The VROP values of the other cases are lower than 1, which means a reinforcing effect.

In summary, regardless of a reinforcing or a weakening effect, the 4-6-8-2 nanoparticle arrangement exerts the most remarkable influence on changing the phase morphologies of the miktoarm PS-*b*-PMMA copolymers at both lower and higher temperature generally, except 13214-type copolymer.

Special Miktoarm PS-*b*-PMMA Copolymer: 13214-Type

Owing to the dramatically different *P* and VROP orders from the other cases, for 13214-type copolymer induced by nanoparticles' doping, it is necessary to investigate such special miktoarm PS-*b*-PMMA copolymer deeply.

We can detect the particularity in the architecture and property of 13214-type copolymer, whose scheme is two times large as it in the subfigure a3 shown in Figure 1: first, the block ratio of PS to PMMA is 1 : 4, which has the highest PMMA percentage of 12 copolymers; second, each joint has two PMMA blocks, four PMMA blocks in total, which could provide much more

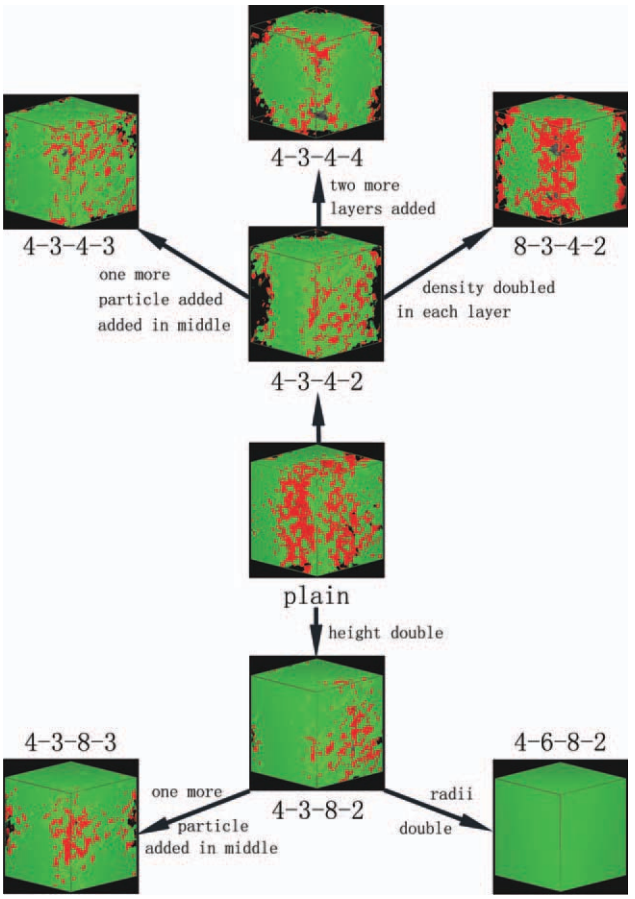

Figure 6. Isodensity surfaces of 13214-type PS-*b*-PMMA copolymer doped with seven kinds of nanoparticles at 413 K. Red represents PS component; green PMMA. [Color figure can be viewed in the online issue, which is available at wileyonlinelibrary.com.]

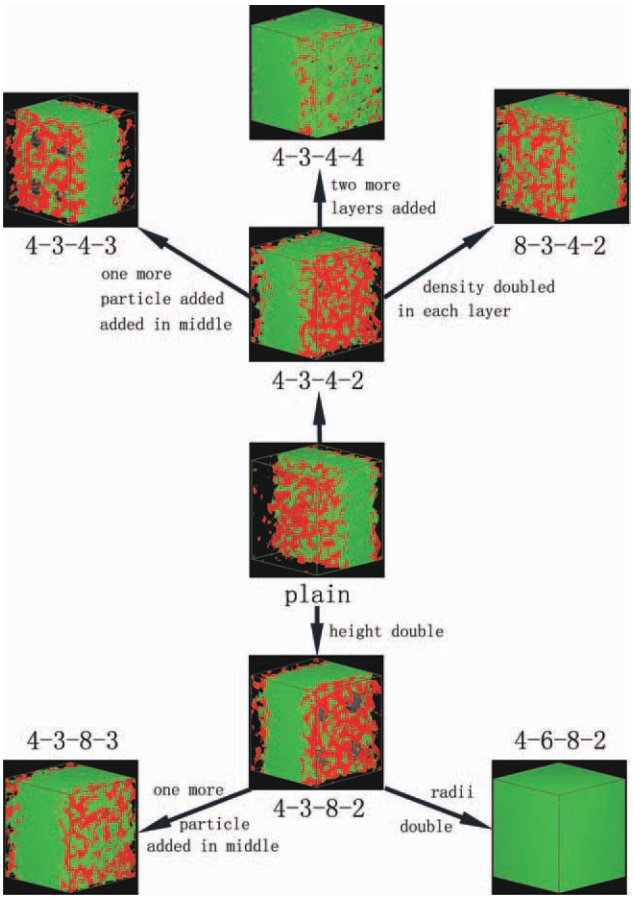

Figure 7. Isodensity surfaces of 13214-type PS-*b*-PMMA copolymer doped with seven kinds of nanoparticles at 443 K. Red represents PS component; green PMMA. [Color figure can be viewed in the online issue, which is available at wileyonlinelibrary.com.]

opportunity for copolymer to "meet" with the same blocks, further form PMMA-rich region; third, such rigid structure-like PS block locates in the middle of copolymer could force the PMMA blocks to extend outside, further increase the "meeting opportunity" during adjusting its placement and orientation, even largen the congregating area; fourth, rigid phenyl of PS block could help the PMMA blocks located at both ends to distribute more dispersedly, which can improve its congregating change.

Figures 5–7 show the mesoscopic simulation results of 13214-type copolymer induced by seven nanoparticle arrangements at 383, 413, and 443 K, respectively. We can see the transition in phase morphology clearly. The cases present local phase separation owing to adding nanoparticles, especially at higher temperature, such as 443 K, and they present as lamellar phase morphologies.

CONCLUSIONS

We study the phase morphologies of plain miktoarm PS-*b*-PMMA copolymers via MesoDyn simulation. It shows that the values of *P* at higher temperature such as 413 and 443 K are nearly the same, but are a lot different from it at lower temperature such as 383 K. For the PMMA-rich copolymers, such as in Groups 2 and 3 could present nearly the same *P*-values at such three temperatures. Furthermore, the architecture of copolymer is vital factor, compared with the chain length.

We investigate the plain miktoarm PS-*b*-PMMA copolymers doped with nanoparticles of various size, densities, and arrangements via mesoscopic simulations. The simulation results show that doping with nanoparticles is a good way of improving the degree of order of the microscopic phases. A more orderly phase morphology can be obtained by increasing the density, size, and number of nanoparticles used as dopant. Among these, increasing the size and the number of the nanoparticles is the top two most efficient methods of enhancing the orderly phase morphologies. The isosurface pictures show that the 13214-type copolymers doped with regardless of any kind of nanoparticles arrangement all present lamellar phase morphologies at 443 K.

ACKNOWLEDGMENTS

This work is supported by the Science-Technology Foundation for Middle-Aged and Young Scientists of Shandong Province (BS2010CL048, BS2011SF026), a Shandong Province Higher School Science & Technology Fund Planning Project (J10LA61), and a Zaozhuang Scientific and Technological Project (200924-2).

REFERENCES

1. Bucknall, D. G., Anderson, H. L. *Science* **2003,** *302*, 1904.
2. Pitsikalis, M., Pispas, S., Mays, J. W., Hadjichristidis, N. *Adv. Polym. Sci.* **1998,** *135*, 1.
3. Mansky, P., Chaikin, P., Thomas, E. L. *J. Mater. Sci.* **1995,** *30*, 1987.
4. Mansky, P., Harrison, C. K., Chaikin, P. M., Register, R. A., Yao, N. *Appl. Phys. Lett.* **1996,** *68*, 2586.
5. Park, M., Harrison, C. K., Chaikin, P. M., Register, R. A., Adamson, D. H. *Science* **1997,** *276*, 1401.
6. Herrninghaus, S., Jacobs, K., Mecke, K., Bischof, J., Fery, A., Ibn-Elfraj, M., Schlagowski, S. *Science* **1998,** *282*, 916.
7. Averopoulos, A., Chan, VZ-H., Lee, V. Y., No, D., Miller, R. D., Hadjichristidis, N., Thomas, N. L. *Chem. Mater* **1998,** *10*, 2109.
8. Thurn-Albrecht, T., Schotter, J., Kastle, A., Emley, N., Shibauchi, T., Krusin-Elbaum, L., Guarini, K., Black, C. T., Tuominen, M. T., Russell, T. P. *Science* **2000,** *290*, 2126.
9. Thurn-Albrecht, T., Steiner, R., DeRouchey, J., Stafford, C. M., Huang, E., Ball, M., Tuominen, M., Hawker, C. J., Russell, T. P. *Adv. Mater.* **2000,** *12*, 787.
10. Black, C. T., Guarini, K. W., Milkove, K. R., Baker, S. M., Tuominen, M. T., Russell, T. P. *Appl. Phys. Lett.* **2001,** *79*, 409.
11. Valls, O. T., Farrell, J. E. *Phys. Rev. E.* **1993,** *47*, R36.
12. Ramirez-Piscina, L., Hernandéz-Machado, A., Sancho, J. M. *Phys. Rev. B.* **1993,** *48*, 125.
13. Kawakatsu, T., Kawasaki, K., Furusaka, M., Okabayashi, H., Kanaya, T. *J. Chem. Phys.* **1993,** *99*, 8200.

14. Shinozaki, A., Oono, Y. *Phys. Rev. E.* **1993,** *48*, 2622.
15. Fraaije, J. E. M. *J. Chem. Phys.* **1993,** *99*, 9202.
16. Fraaije, J. G. E. M., van Vlimmeren, B. A. C., Maurits, N. M., Postma, M., Evers, O. A., Hoffman, C., Altevogt, P., Goldbeck-Wood, G. *J. Chem. Phys.* **1997,** *106*, 4260.
17. Jawalkar, S. S., Adoor, S. G., Sairam, M., Nadagouda, M. N., Aminabhavi, T. M. *J. Phys. Chem. B.* **2005,** *109*, 15611.
18. Mu, D., Huang, X. R., Lu, Z. Y., Sun, C. C. *Chem. Phys.* **2008,** *348*, 122.
19. Mu, D., Li, J. Q., Wang, S. *J. Appl. Polym. Sci.* **2011,** *119*, 265.
20. Mu, D., Li, J. Q., Zhou, Y. H. *J. Mol. Model* **2011,** *17*, 607.
21. Mu, D., Li, J. Q., Wang, S. *J. Appl. Polym. Sci* **2011,** *122*, 64.
22. Mu, D., Li, J. Q., Li, W. D., Wang, S. *J. Mol. Model, to appear.*
23. Paul, D. R., Newman, S. Polymer Blends; Academic Press: New York, **1978.**
24. Abd-El-Messieh, S. L. *Polym. Plast. Technol. Eng.* **2003,** *42*, 153.
25. Schneider, I. A., Calugaru, E. M. *Eur. Polym. J.* **1976,** *12*, 879.
26. Bada, R., Perez, Jubindo, M. A., De, L. A., Fuente, M. R. *Mater. Chem. Phys.* **1987,** *18*, 359.
27. Zhu, P. P. *Eur. Polym. J.* **1997,** *33*, 411.
28. Lee, J. K., Han, C. D. *Polymer* **1999,** *40*, 6277.
29. Lee, C. F. *Polymer* **2000,** *41*, 1337.
30. Li, X., Han, Y. C., An, L. J. *Polymer* **2003,** *44*, 8155.
31. Walheim, S., Boltau, M., Mlynek, J., Krausch, G., Steiner, U. *Macromolecules* **1997,** *30*, 4995.
32. Schmidt, J. J., Gardella, J. A., Jr.; Salvati, L. *Macromolecules* **1989,** *22*, 4489.
33. Bucknall, D. G., Anderson, H. L. *Science* **2003,** *302*, 1904.
34. Matsen, M. W., Schick, M. *Phys. Rev. Lett.* **1994,** *72*, 2660.
35. Chen, J. T., Thomas, E. L., Ober, C. K., Mao, G. *Science* **1996,** *273*, 343.
36. Jenekhe, S. A., Chen, X. L. *Science* **1998,** *279*, 1903.